Complete characterization of the spasing (L-L) curve of a three-level quantum coherence enhanced spaser for design optimization

Lakshitha Kumarapperuma,[1,a)] Malin Premaratne,[1,a)] Pankaj K. Jha,[2] Mark I. Stockman,[3] and Govind P. Agrawal[4]
[1]*Advanced Computing and Simulation Laboratory (AχL), Department of Electrical and Computer Systems Engineering, Monash University, Clayton, Victoria 3800, Australia*
[2]*Department of Mechanical Engineering, University of California, Berkeley, California 94720, USA*
[3]*Department of Physics and Astronomy, Georgia State University, Atlanta, Georgia 30303 USA*
[4]*The Institute of Optics, University of Rochester, Rochester, New York 14627, USA*

(Received 8 February 2018; accepted 5 May 2018; published online 17 May 2018)

We demonstrate that it is possible to derive an approximate analytical expression to characterize the spasing (L-L) curve of a coherently enhanced spaser with 3-level gain-medium chromophores. The utility of this solution stems from the fact that it enables optimization of the large parameter space associated with spaser designing, a functionality not offered by the methods currently available in the literature. This is vital for the advancement of spaser technology towards the level of device realization. Owing to the compact nature of the analytical expressions, our solution also facilitates the grouping and identification of key processes responsible for the spasing action, whilst providing significant physical insights. Furthermore, we show that our expression generates results within 0.1% error compared to numerically obtained results for pumping rates higher than the spasing threshold, thereby drastically reducing the computational cost associated with spaser designing. *Published by AIP Publishing.* https://doi.org/10.1063/1.5025354

The ability to confine and manipulate light on the nano-scale enables the development of ultra-fast, efficient and miniaturized optical circuits and systems, leading to many applications in nanotechnology.[1–5] Owing to the advancements in sophisticated nano-fabrication techniques, device sizes approaching tens of nanometers have been built and tested reliably.[6] However, miniaturization of optical devices below the sub-wavelength scale has been constrained by the fundamental limit of diffraction.[7] Therefore, confinement of light to unprecedentedly smaller volumes is essential for enabling very strong light-matter interactions in order to realize ultra-fast nano-scale optical devices. These challenges have been met successfully in the emerging field of quantum nano-plasmonics with the use of Surface Plasmons (SPs).[2,8–12] Generally, SPs are excited at metal-dielectric interfaces and as a result, they naturally experience intrinsic losses.[13] Therefore, energy must be transferred from an external source in order to replenish and sustain SP resonances.[8]

Coherent amplification of localized SPs via stimulated emission, theorized by Stockman and Bergman in 2003,[14] led to the discovery of spaser (Surface Plasmon Amplification by Stimulated Emission of Radiation) which is the nano-scale counterpart of laser. The effect of spasing was first demonstrated experimentally by Noginov *et al.* in 2009.[15] Since then, developing efficient, reliable and easily controllable spasers has become one of the major research areas in nano-plasmonics.[16–19]

A typical spaser consists of a plasmonic resonator (similar to the laser cavity) that supports SP modes and a gain medium that supplies energy to amplify them. Usually, the gain medium chromophores are modelled as two level systems effectively, which have only one mode of external input in the form of an incoherent pump.[20] The intensity of the output optical field of a spaser can be represented by the number of localized SPs generated per spasing mode. These output characteristics of spasers are known as spasing curves[20] (a counterpart of the L-L curve for lasers[7]).

Due to the gain saturation caused by the plasmonic feedback on the gain medium chromophores, spasers generate fewer number of SPs while having higher thresholds. Dorfman *et al.*[21] have significantly improved the output efficiency of spasers by introducing another coherent optical field as an input to control the spaser output characteristics. They utilize a concept very much analogous to lasing without inversion (LWI) to enhance spaser performance. The chromophores in this scenario have been modelled as 3-level systems.

Owing to the number of coupled equations in this formulation, the equations naturally lend themselves to numerical solutions. However, an analytical solution closely approximating the exact numerical solution may not only provide valuable insights but may also contribute towards design optimization. Therefore, in this letter, we derive an analytical expression for the spasing curve of a spaser with 3-level gain medium chromophores. We have established the accuracy of the derived expression by comparing our results with detailed numerical simulations.

The basic configuration and the energy flow diagram of our system are illustrated in Fig. 1. A plasmonic nanostructure is surrounded by an optical gain medium which comprises homogeneously distributed generic 3-level quantum emitters. An emitter has a ground state ($|1\rangle$), as well as two excited states ($|2\rangle$ and $|3\rangle$). The two inputs to the spaser are denoted by the incoherent pumping rate g (coupled to the transition $|1\rangle \rightarrow |3\rangle$) and the Rabi Frequency of the coherent

a)Authors to whom correspondence should be addressed: lakshitha.kumarapperuma@monash.edu and malin.premaratne@monash.edu

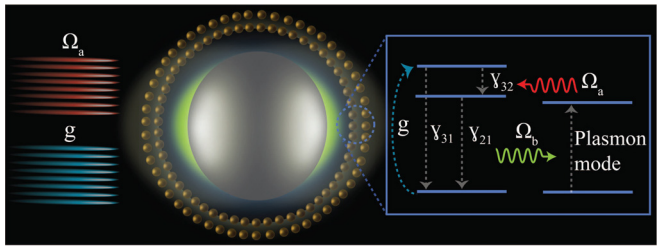

FIG. 1. Basic operation of a SPASER: Gain medium chromophores are excited using an incoherent pump (g) as well as a coherent drive Ω_a. The transition $|2\rangle \rightarrow |1\rangle$ is coupled to one of the SP modes in the plasmonic nano-structure, which excites SPs via stimulated emission.

input field Ω_a (coupled to the transition $|2\rangle \rightarrow |3\rangle$). Since we are interested in the continuous wave (CW) operation of the spaser, g and Ω_a will be provided continuously as long as the spaser works, in order to sustain the SPs. The spasing transition $|2\rangle \rightarrow |1\rangle$ represented by the corresponding Rabi frequency Ω_b is coupled with a surface plasmon mode in the nano-plasmonic resonator to transfer energy non-radiatively from the chromophores to the SPs, thereby sustaining the spasing process. The plasmonic field generated in the nano-structure provides an internal feedback to the gain medium during operation. The spontaneous decay rates in the 3-level emitters are denoted by γ_{21}, γ_{32} and γ_{31}, as indicated in Fig. 1. The total number of 3-level quantum emitters (chromophores) in the gain medium is denoted by N_c.

To simplify our analysis, we approximate the 3-level emitters as dipoles.[16] Rotating Wave Approximation (RWA) has been deployed to neglect the rapidly oscillating terms in the Hamiltonian.[7] Then, the total Hamiltonian of the gain medium in the interaction picture can be written as

$$\mathcal{H}_{int} = \Sigma_p\{-\hbar\Delta_b^{(p)}|1\rangle\langle 1| + \hbar\Delta_a^{(p)}|3\rangle\langle 3| - (\hbar\Omega_b^{(p)}|2\rangle\langle 1| + \hbar\Omega_a^{(p)}|3\rangle\langle 2| + c.c)\}, \quad (1)$$

where $c.c.$ denotes the complex conjugate and $\hbar$ is the reduced Planck's constant. The Hamiltonian takes into account the summation of all the N_c chromophores and is denoted by Σ_p. We assume that the inter-chromophore interactions are comparatively weak enough to be neglected when writing the Hamiltonian.[7,16,20] In Eq. (1), detunings are defined as $\Delta_a = \omega_{32} - \omega_a$ and $\Delta_b = \omega_{21} - \omega_b$,[22] where ω_{32} and ω_{21} are the frequencies of the corresponding band gaps of the chromophores and ω_a and ω_b are defined as the frequencies of the coherent field and the plasmonic field, respectively.

Standard semiclassical theory has been adopted in the analysis, where the gain medium is treated quantum-mechanically and the SPs as well as photons are treated as classical quantities.[20,21] Therefore, we express both the plasmon annihilation operator, $\hat{a}_n$, and the photon annihilation operator, $\hat{b}_m$, as time varying complex numbers (C-numbers) with definitions $a_n = a_{0_n}e^{-i\omega_s t}$ and $b_m = b_{0_m}e^{-i\omega_{32}t}$.[16] a_{0_n} and b_{0_m} are slowly varying amplitudes, whereas ω_s is the frequency related to spasing. Based on the above information, the number of SPs per n^{th} spasing mode can be expressed as $N_n = |a_{0_n}|^2$.[7] $\Omega_b^{(p)}$ is expressed as $-A_n d_{21}^{(p)}\nabla\psi_n a_{0_n}/\hbar$, where $A_n = (\{4\pi\hbar\mathrm{Re}[s(\omega_n)]\}/\{\epsilon_d\mathrm{Re}[ds(\omega_n)/d\omega_n]\})^{1/2}$. Here, $s(\omega_n) = \epsilon_d/[\epsilon_d - \epsilon_m(\omega_n)]$, where ϵ_d is the bath permittivity and $\epsilon_m(\omega_n)$ is the permittivity of the metal at plasmon resonance frequency ω_n. The dipole moment element of the gain chromophores is given by d_{21} and the gradient of the potential function $\nabla\psi_n \approx 1/\sqrt{V}$, where V is the modal volume of the electric field generated by the plasmon mode, which is directly related to the size and the shape of the nano-particle.[21,23] Furthermore, Ω_a is considered a constant since we assume that the driving field is strong enough to maintain the number of photons in mode m constant under operating conditions.[21]

The p^{th} gain medium chromophore is modelled as an open quantum system using the Liouville-von Neumann master equation, $\dot{\rho}^{(p)} = -i/\hbar[\mathcal{H}_{int}, \rho^{(p)}] - \mathcal{L}\rho^{(p)}$, where $\dot{\rho}^{(p)}$ represents the time derivative of the density matrix. $\mathcal{L}$ is the Lindblad super-operator that quantifies the interactions with the environment, such as spontaneous decay of the gain medium, incoherent pumping and dephasing (decoherence).[24] Lindblad terms have been extracted from Ref. 21, 25, and 26. The off-diagonal relaxation rates are $\Gamma_{21} = 0.5(\gamma_{21} + g) + \gamma_{ph} + i\Delta_b$, $\Gamma_{31} = 0.5(\gamma_{31} + \gamma_{32} + g) + \gamma_{ph} + i(\Delta_a + \Delta_b)$ and $\Gamma_{32} = 0.5(\gamma_{31} + \gamma_{32} + \gamma_{21}) + \gamma_{ph} + i\Delta_a$, where γ_{ph} is the dephasing (decoherence) rate of ρ_{ij}.[21] Hence, the emitter density matrix elements ρ_{ij} are given by the following complex valued coupled partial differential equations:

$$\dot{\rho}_{11} = \gamma_{21}\rho_{22} + \gamma_{31}\rho_{33} - g\rho_{11} + i(\Omega_b^*\rho_{21} - \Omega_b\rho_{21}^*), \quad (2a)$$

$$\dot{\rho}_{33} = -(\gamma_{31} + \gamma_{32})\rho_{33} + g\rho_{11} - i(\Omega_a^*\rho_{32} - \Omega_a\rho_{32}^*), \quad (2b)$$

$$\dot{\rho}_{21} = -\Gamma_{21}\rho_{21} - i\Omega_b(\rho_{22} - \rho_{11}) + i\Omega_a^*\rho_{31}, \quad (2c)$$

$$\dot{\rho}_{31} = -\Gamma_{31}\rho_{31} - i\Omega_b\rho_{32} + i\Omega_a\rho_{21}, \quad (2d)$$

$$\dot{\rho}_{32} = -\Gamma_{32}\rho_{32} - i\Omega_a(\rho_{33} - \rho_{22}) - i\Omega_b^*\rho_{31}, \quad (2e)$$

$$\rho_{11} = 1 - \rho_{22} - \rho_{33}. \quad (2f)$$

We describe the stimulated emission of SPs as their excitation by the coherent polarization of the gain medium corresponding to the transition $|2\rangle \rightarrow |1\rangle$. Therefore, the time evolution of the plasmon annihilation operator should be of the same form as that of a 2-level gain medium,[16] which is expressed by invoking the Heisenberg equation of motion for a_{0_n} as

$$\dot{a_{0_n}} = -\Gamma_n a_{0_n} + i\Sigma_p\rho_{21}^{(p)}\tilde{\Omega}_b^{(p)}. \quad (3)$$

The SP relaxation rate Γ_n is expressed as $\gamma_n + i\Delta_n$, where γ_n is the plasmon decay rate and Δ_n is the detuning between ω_n and the frequency of the $|2\rangle \rightarrow |1\rangle$ transition (ω_{21}). The value $\tilde{\Omega}_b^{(p)}$ is the single plasmon Rabi frequency denoted by $\tilde{\Omega}_b^{(p)} = \Omega_b^{(p)}/a_{0_n}$. Next, we assume that all N_c chromophores interact with the SPs identically, and hence we omit the index p and set $\Sigma_p \rightarrow N_c$ in Eq. (3).

Next, by writing the complex variables and coefficients in Eqs. (2a)–(2f) and Eq. (3) in the form of $z = \mathrm{Re}(z) + i\mathrm{Im}(z)$ and by equating the real and imaginary parts of the equations separately, we derive a set of real valued, non-linear, coupled differential Eqs. (4a)–(4k). Note the labeling we have followed: $\mathrm{Re}(\rho_{cd}) = \rho_{cd}^R$, $\mathrm{Im}(\rho_{cd}) = \rho_{cd}^I$, $\mathrm{Re}(a_{0_n}) = \mathcal{A}$ and $\mathrm{Im}(a_{0_n}) = \mathcal{B}$. Furthermore, Δ_a and Δ_b are taken as zero since

resonant coupling is assumed between relevant interactions. Hence, all Γ_{cd}s are assumed real.[16,21]

$$\dot{\rho}_{11} = \gamma_{21}\rho_{22} + \gamma_{31}\rho_{33} - g\rho_{11} + 2\tilde{\Omega}_b(B\rho_{21}^R - A\rho_{21}^I), \quad (4a)$$

$$\dot{\rho}_{33} = -(\gamma_{31} + \gamma_{32})\rho_{33} + g\rho_{11} + 2\Omega_a\rho_{32}^I, \quad (4b)$$

$$\dot{\rho}_{21}^R = -\Gamma_{21}\rho_{21}^R + \tilde{\Omega}_b B\rho_{22} - \tilde{\Omega}_b B\rho_{11} - \Omega_a\rho_{31}^I, \quad (4c)$$

$$\dot{\rho}_{21}^I = -\Gamma_{21}\rho_{21}^I - \tilde{\Omega}_b A\rho_{22} + \tilde{\Omega}_b A\rho_{11} - \Omega_a\rho_{31}^R, \quad (4d)$$

$$\dot{\rho}_{31}^R = -\Gamma_{31}\rho_{31}^R + \tilde{\Omega}_b A\rho_{32}^I + \tilde{\Omega}_b B\rho_{32}^R - \Omega_a\rho_{21}^I, \quad (4e)$$

$$\dot{\rho}_{31}^I = -\Gamma_{31}\rho_{31}^I - \tilde{\Omega}_b A\rho_{32}^R + \tilde{\Omega}_b B\rho_{32}^I + \Omega_a\rho_{21}^R, \quad (4f)$$

$$\dot{\rho}_{32}^R = -\Gamma_{32}\rho_{32}^R + \tilde{\Omega}_b A\rho_{31}^I - \tilde{\Omega}_b B\rho_{31}^R, \quad (4g)$$

$$\dot{\rho}_{32}^I = \Omega_a(\rho_{22} - \rho_{33}) - \Gamma_{32}\rho_{32}^I - \tilde{\Omega}_b(A\rho_{31}^R - B\rho_{31}^I), \quad (4h)$$

$$\rho_{11} = 1 - \rho_{22} - \rho_{33}, \quad (4i)$$

$$\dot{\mathcal{A}} = -\gamma_n\mathcal{A} + \Delta_n\mathcal{B} - N_c\tilde{\Omega}_b\rho_{21}^I, \quad (4j)$$

$$\dot{\mathcal{B}} = -\gamma_n\mathcal{B} - \Delta_n\mathcal{A} + N_c\tilde{\Omega}_b\rho_{21}^R. \quad (4k)$$

$N_n = |a_{0_n}|^2$ and $|a_{0_n}|^2 = \mathcal{A}^2 + \mathcal{B}^2$. Surface plasmons are modelled using C-numbers corresponding to bosonic number state representation, where N_n denotes the expected number of SPs generated in the spasing mode with frequency ω_n.[27] The total energy output of the spaser is then given by $\hbar\omega_n \times N_n$. Hence, N_n gives a measure of the total output energy of the spaser. So, our aim is to simultaneously solve Eqs. (4a)–(4k) and derive an analytical expression for N_n. Such an expression would not only reduce the computational burden of calculating the output energy ($\propto N_n$) of the spaser,[7] but would also provide numerous advantages for design optimization, whilst providing valuable physical insights into the operation of the device.

To study these Eqs. (4a)–(4k) in detail and observe the time evolution of ρ_{cd}, $\mathcal{A}$ and $\mathcal{B}$, we carry out some indicative numerical simulations. A silver nano-sphere of radius 40 nm is used as the plasmonic nano-structure. All parameter values are taken from Ref. 20, 21, 28, and 29, where $\omega_n = 2.5\,\text{eV}$, $\gamma_n = 5.3 \times 10^{14}\text{s}^{-1}$, $\Delta_n = 3.2 \times 10^{12}\text{s}^{-1}$, $\gamma_{21} = 4 \times 10^{12}\text{s}^{-1}$, $\gamma_{32} = 4 \times 10^{11}\text{s}^{-1}$, $\gamma_{31} = 4 \times 10^{10}\text{s}^{-1}$, $N_c = 6 \times 10^4$ and $\epsilon_d = 2.25$. The bulk permittivity values of silver are obtained from the Johnson and Christy model.[28] The time evolution of $\mathcal{A}$ is given in Fig. 2 for an incoherent pumping rate (g) of $24 \times 10^{12}\text{s}^{-1}$. Due to the inherent slowly varying nature of the C-numbers (a_{0_n} and ρ_{cd}s for $c \neq d$),[20] multiple rounds of detailed numerical simulations show that all time derivatives

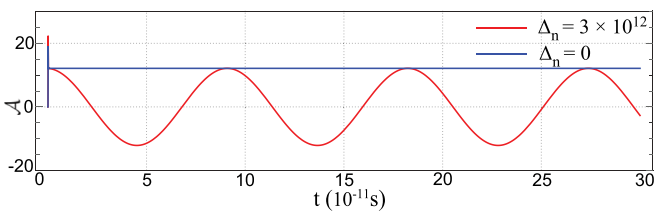

FIG. 2. Time evolution of $\mathcal{A}$ when $\Delta_n = 0$ and $\Delta_n = 3 \times 10^{12}\text{s}^{-1}$. When the spasing transition ($|2\rangle \rightarrow |1\rangle$) is resonantly coupled with the SP mode, the complex number representation of the plasmon annihilation operator (a_{0_n}) after the initial transients becomes constant over time. When there is significant detuning (i.e., $\Delta_n \neq 0$), a_{0_n} varies sinusoidally over time.

in Eqs. (4a)–(4k) do not become zero simultaneously, even in the steady state for any g or Ω_a. Since $\Delta_n \ll \gamma_n, \omega_n$, we now assume that the $|2\rangle \rightarrow |1\rangle$ transition and the SP mode are resonantly coupled (i.e., $\Delta_n = 0$) and carry out the same set of numerical simulations. Note that such an assumption is physically justifiable as well, since the system designers always strive to achieve near or perfectly resonant coupling. The time evolution of $\mathcal{A}$ when $\Delta_n = 0$ is given in Fig. 2, where $\mathcal{A}$ becomes constant in the steady state, unlike when $\Delta_n \neq 0$. This is the same for all other variables (ρ_{cd} and $\mathcal{B}$) for all combinations of g, Ω_a and system parameters. Therefore, it is possible to set all time derivatives in Eqs. (4a)–(4k) to 0, which yields a set of algebraic equations that can be solved. By simultaneously solving the system of nonlinear algebraic equations, we derive the full explicit analytical expression for N_n as follows:

$$N_n = [(-8\gamma_n\mathcal{F}_5((\Gamma_{21}\Gamma_{31}\gamma_n + \gamma_n\Omega_a^2)\mathcal{F}_{10} + N_c\tilde{\Omega}_b^2(\Gamma_{31}\Gamma_{32}\mathcal{F}_4 + \Omega_a^2\mathcal{F}_7)) + \mathcal{F}_8^2)^{\frac{1}{2}} - \mathcal{F}_8]\frac{1}{\mathcal{F}_9}, \quad (5)$$

where $\mathcal{F}_1 = \Gamma_{32}(2\gamma_{31} + 2\gamma_{32} + g) + 6\Omega_a^2$, $\mathcal{F}_2 = \gamma_{21}(\gamma_{31} + \gamma_{32} + g) + \gamma_{32}g$, $\mathcal{F}_3 = \gamma_{21} - 3\gamma_{31} - \gamma_{32} - 3g$, $\mathcal{F}_4 = \gamma_{21}\gamma_{31} + \gamma_{21}\gamma_{32} - \gamma_{32}g$, $\mathcal{F}_5 = 2\gamma_{31} + 2\gamma_{32} + g$, $\mathcal{F}_6 = \gamma_{21} + \gamma_{31} + 2g$, $\mathcal{F}_7 = 2\gamma_{31}\Gamma_{31} - 2\Gamma_{31}g + 2\Gamma_{31}\gamma_{21} - \gamma_{21}g$, $\mathcal{F}_8 = 2\gamma_n\Gamma_{31}\mathcal{F}_1 + \gamma_n\Gamma_{21}\mathcal{F}_2 + 2\gamma_n\Omega_a^2\mathcal{F}_3 + N_c\tilde{\Omega}_b^2\mathcal{F}_4$, $\mathcal{F}_9 = 4\gamma_n\mathcal{F}_5\tilde{\Omega}_b^2$ and $\mathcal{F}_{10} = \Gamma_{32}\mathcal{F}_2 + 2\Omega_a^2\mathcal{F}_6$. Equation (5) can be used to analyze the number of SPs analytically, for $g > g_{th}$, where g_{th} is the spasing threshold. It gives a fully analytical characterization of the spasing curve since it contains both controlling parameters g and Ω_a as well as all system specific parameters. We now compare the numerical simulations with the results generated by our analytical expression for the spaser proposed in Ref. 21. The error percentage ($\mathcal{E}$) is defined as $(N_n^s - N_n)/N_n^s \times 100\%$, where N_n^s is the value obtained in numerical simulations. Figures 3(a) and 3(b) depict the spasing curve of N_n as g varies. Different curves have been obtained for various values of Ω_a. It is evident that $\mathcal{E}$ for the whole spasing regime ($g > g_{th}$) remains less than 0.1% in all practical cases.[16–18,20] Studying the effect of dephasing (decoherence) on spasing is also of utmost importance for complete characterization.[24] Therefore, another comparison is made in Figs. 3(c) and 3(d) to investigate the effect of decoherence (γ_{ph}) on spasing. While it becomes evident that the robustness of the spaser output against decoherence has been enhanced as Ω_a is increased, it can also be seen that Eq. (5) can be used with an acceptable accuracy ($\mathcal{E} < 0.1\%$) to study the effect of dissipative processes such as decoherence (γ_{ph}) in a spaser.

We have ideally assumed a pure state initial condition for the density matrix elements when obtaining numerical results.[21,22] There is a slight disagreement between the numerical and analytical results for very small g values above the threshold for high Ω_a. This could be due to the inability of the system to produce the expected response to high Ω_a values at very low pumping rates, as the number of electrons in high energy levels is minute in the initial spasing build up. If a more practical mixed initial state is assumed instead,[2,8] even this slight disagreement will no longer be

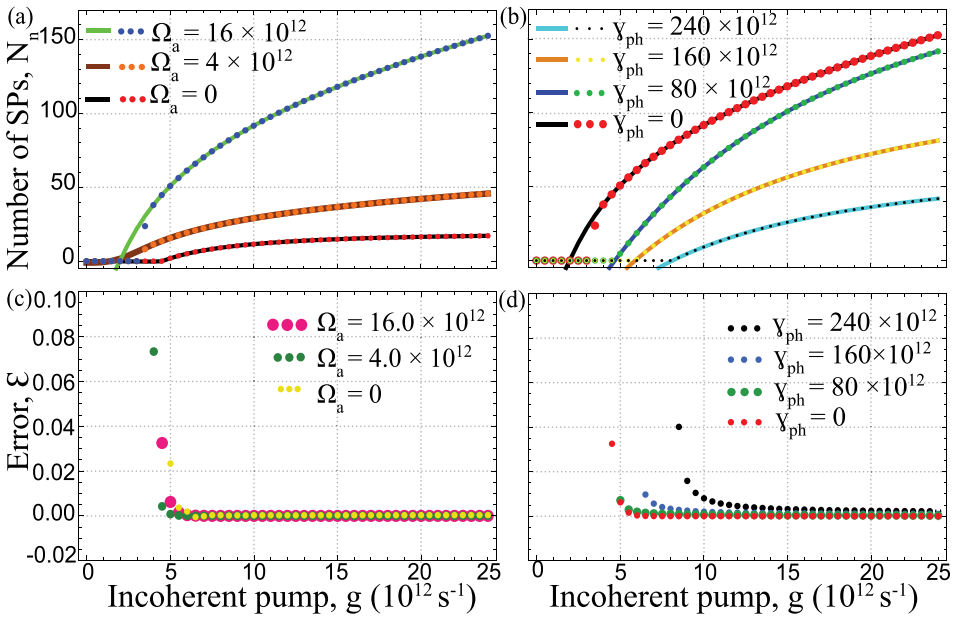

FIG. 3. (a)–(d) compare the spasing curves obtained both numerically and analytically. Dotted lines in (a) and (c) represent the numerical results and the solid lines represent our analytical results. (a) The spasing curves obtained both numerically and analytically for different values of Ω_a, where $\gamma_{ph} = 0$ for all cases. The corresponding error ($\mathcal{E}$) values are shown in (c). (b) The spasing curves obtained both numerically and analytically for different values of γ_{ph}, where $\Omega_a = 16 \times 10^{12}\text{s}^{-1}$ for all cases. The corresponding error ($\mathcal{E}$) values are shown in (d). Percentage error ($\mathcal{E}$) is less than 0.1% for all cases in the spasing regime ($g > g_{th}$).

present due to the initial presence of electrons in the upper energy levels to compensate for the low pumping rates. Furthermore, for practical pumping rates so far reported in the literature ($g > 5 \times 10^{12}\,\text{s}^{-1}$),[16–18,20] the values obtained using both types of initial conditions converge to our steady state analytical solution.

Figures 3 and 4 also suggest that apart from accurately characterizing the spaser output with $\mathcal{E} < 0.1\%$ for $g > g_{th}$ when $\Delta_n \ll \gamma_n, \omega_n$, it is also possible to use Eq. (5) to qualitatively understand the threshold conditions (g_{th}) by setting $N_n = 0$. When Δ_n is comparable or greater than ω_n or γ_n, the predicted analytical values will not be within the accepted error bounds, i.e., $\mathcal{E} > 0.1\%$. But such off-resonant conditions are not desired practically from a system designer's perspective since such conditions do not facilitate efficient energy transfer and there is some likelihood for system instability as well.[7]

Equation (5) can be tailored for different nanoparticles and gain media by varying $\tilde{\Omega}_b$, decay and dephasing rates and N_c accordingly. It is also possible to derive simpler expressions when the parameters are constrained to specific regimes. For example, if a certain spaser configuration satisfies the condition $g > \gamma_{21} \gg \gamma_{32} \gg \gamma_{31}$, its spasing curve can be derived in a more simplified form as follows:

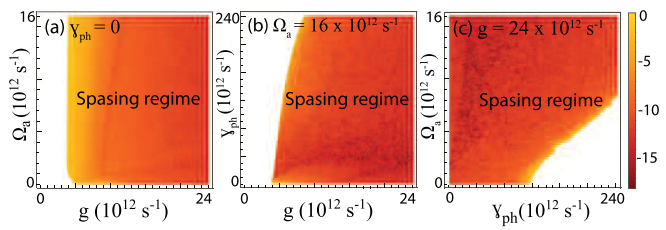

FIG. 4. (a)–(c) depict the two-dimensional plots for the logarithmic value of the absolute value of the error ($\mathcal{E}$) percentage. (a) $\log_{10}(|\mathcal{E}|)$ for a range of values of g and Ω_a when $\gamma_{ph} = 0$. (b) $\log_{10}(|\mathcal{E}|)$ for a range of values of g and γ_{ph} when $\Omega_a = 16 \times 10^{12}\text{s}^{-1}$. (c) $\log_{10}(|\mathcal{E}|)$ for a range of values of Ω_a and γ_{ph} when $g = 24 \times 10^{12}\text{s}^{-1}$. Error ($\mathcal{E}$) is less than 0.1% for all cases in the spasing regime. Non-spasing regimes are shown in white.

$$N_n \approx \frac{\gamma_{32}N_c}{4\gamma_n}\left(1 - \frac{\gamma_{21}}{g}\right) - \frac{\gamma_{21}}{4\tilde{\Omega}_b^2}\left(g + \frac{2\Omega_a^2}{g}\right) + \frac{1}{4}\left[\left(1 - \frac{\gamma_{21}}{g}\right)^2\left(\frac{\gamma_{32}N_c}{\gamma_n}\right)^2 + \frac{8gN_c\Omega_a^2}{\gamma_n}\right]^{\frac{1}{2}}. \quad (6)$$

To simply model the main physical dependencies of the system, we considered the Taylor series expansion of Eq. (5) for the whole operating regime for fixed values of Ω_a. We could approximate that N_n shows a logarithmic behavior as g varies, expressed as $k_1 \ln(g - k_2 g_{th})$, where k_1 and k_2 depend on system parameters and Ω_a. Similar analyses can be done to simply approximate the relationships between other parameters.

Equation (5) can be used to analytically study the relationship between any selected pair of parameters by setting others as constants, similar to the way it is done for g vs. N_n. To demonstrate the versatility of our solution, we have studied how N_n behaves as the number of chromophores (N_c) is varied in Fig. 5(a). Then, we set $N_n = 0$ in Eq. (5) and express the threshold number of chromophores $N_{c,th}$ as a function of Ω_a, depicted in Fig. 5(b). Such analyses for any set of parameters can be performed using our analytical solution. This enables the system designers to develop highly intuitive and methodical optimization schemes for physically meaningful parameter sets, which are much simpler than full-blown numerical approaches. In addition, by setting

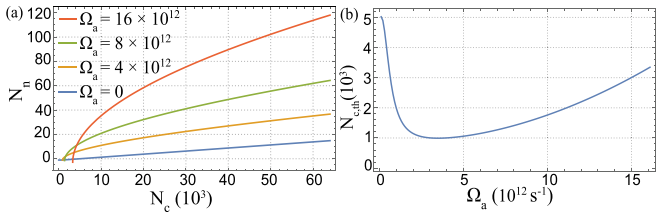

FIG. 5. (a) Depicts the variation of N_n as N_c varies for different values of Ω_a. (b) The variation of minimum N_c (threshold) required to start spasing ($N_{c,th}$) as Ω_a varies in the configuration given in (a). Note that $g = 15 \times 10^{12}\,\text{s}^{-1}$ and $\gamma_{ph} = 0$ for both (a) and (b).

$\Omega_a = 0$ and $\gamma_{32} > g$ in Eq. (5) for a much faster $|3\rangle \rightarrow |2\rangle$ population transfer,[21] it is possible to study the spasing output of a 2-level spaser[20] analytically.

In conclusion, we have derived an explicit analytical expression and simpler approximations to describe the spasing curves of a coherently enhanced spaser, whilst providing valuable physical insights into the operation of the spaser. The method we have followed in deriving the solution itself will aid similar nanoplasmonic systems to be solved analytically to very high accuracy. The derived expression provides the basis to calculate the optimal system parameters and inputs required in order to achieve desired spasing outputs, which is a capability that surpasses numerical solutions. Therefore, the proposed scheme enables the utilization of spasers in complex nanoplasmonic systems by enabling design optimization. In addition, it grants a faster way to determine the output energy generated by the localized SPs, eliminating the need for computationally expensive numerical simulations. The error of the spasing curve generated by our expression is under 0.1% for the whole operating regime above the spasing threshold, suggesting an almost perfect characterization.

L.K. would like to thank Lahirunie Kahingala, all members of AχL at Monash University and Kasun Fernando of University of Maryland for continued encouragement and insightful discussions.

[1]S. Lal, S. Link, and N. J. Halas, "Nano-optics from sensing to waveguiding," Nat. Photonics **1**, 641–648 (2007).
[2]S. A. Maier, *Plasmonics: Fundamentals and Applications* (Springer Science & Business Media, 2007).
[3]S. Mallawaarachchi, M. Premaratne, S. D. Gunapala, and P. K. Maini, "Tuneable superradiant thermal emitter assembly," Phys. Rev. B **95**, 155443 (2017).
[4]D. Weeraddana, M. Premaratne, and D. L. Andrews, "Direct and third-body mediated resonance energy transfer in dimensionally constrained nanostructures," Phys. Rev. B **92**, 035128 (2015).
[5]S. Mallawaarachchi, S. D. Gunapala, M. I. Stockman, and M. Premaratne, "Generalized superradiant assembly for nanophotonic thermal emitters," Phys. Rev. B **97**, 125406 (2018).
[6]B. Radisavljevic, A. Radenovic, J. Brivio, V. Giacometti, and A. Kis, "Single-layer mos2 transistors," Nat. Nanotechnol. **6**, 147–150 (2011).
[7]M. I. Stockman, "Nanoplasmonics: Past, present, and glimpse into future," Opt. Express **19**, 22029–22106 (2011).
[8]M. Premaratne and G. P. Agrawal, *Light Propagation in Gain Media: Optical Amplifiers* (Cambridge University Press, 2011).
[9]H. A. Atwater and A. Polman, "Plasmonics for improved photovoltaic devices," Nat. Mater. **9**, 205–213 (2010).
[10]H. Hapuarachchi, M. Premaratne, Q. Bao, W. Cheng, S. D. Gunapala, and G. P. Agrawal, "Cavity QED analysis of an exciton-plasmon hybrid molecule via the generalized nonlocal optical response method," Phys. Rev. B **95**, 245419 (2017).
[11]H. P. Hapuarachchi, S. Mallawaarachchi, H. T. Hattori, W. Zhu, and M. Premaratne, "Optoelectronic figure of merit of a metal nanoparticle-quantum dot (MNP-QD) hybrid molecule for assessing its suitability for sensing applications," J. Phys.: Condens. Matter **30**(5), 054006 (2018).
[12]W. Zhu, I. D. Rukhlenko, and M. Premaratne, "Linear transformation optics for plasmonics," J. Opt. Soc. Am. B **29**, 2659–2664 (2012).
[13]W. L. Barnes, A. Dereux, and T. W. Ebbesen, "Surface plasmon subwavelength optics," Nature **424**, 824 (2003).
[14]D. J. Bergman and M. I. Stockman, "Surface plasmon amplification by stimulated emission of radiation: Quantum generation of coherent surface plasmons in nanosystems," Phys. Rev. Lett. **90**, 027402 (2003).
[15]M. Noginov, G. Zhu, A. Belgrave, R. Bakker, V. Shalaev, E. Narimanov, S. Stout, E. Herz, T. Suteewong, and U. Wiesner, "Demonstration of a spaser-based nanolaser," Nature **460**, 1110 (2009).
[16]M. Premaratne and M. I. Stockman, "Theory and technology of spasers," Adv. Opt. Photonics **9**, 79–128 (2017).
[17]C. Rupasinghe, I. D. Rukhlenko, and M. Premaratne, "Spaser made of graphene and carbon nanotubes," ACS Nano **8**, 2431–2438 (2014).
[18]C. Jayasekara, M. Premaratne, S. D. Gunapala, and M. I. Stockman, "Mos_2 spaser," J. Appl. Phys. **119**, 133101 (2016).
[19]B. Liu, W. Zhu, S. D. Gunapala, M. I. Stockman, and M. Premaratne, "Open resonator electric spaser," ACS Nano (2017) **11**(12), 12573–12582.
[20]M. I. Stockman, "The spaser as a nanoscale quantum generator and ultrafast amplifier," J. Opt. **12**, 024004 (2010).
[21]K. E. Dorfman, P. K. Jha, D. V. Voronine, P. Genevet, F. Capasso, and M. O. Scully, "Quantum-coherence-enhanced surface plasmon amplification by stimulated emission of radiation," Phys. Rev. Lett. **111**, 043601 (2013).
[22]P. K. Jha, Y. Wang, X. Ren, and X. Zhang, "Quantum-coherence-enhanced transient surface plasmon lasing," J. Opt. **19**, 054002 (2017).
[23]T. V. Shahbazyan, "Mode volume, energy transfer, and spaser threshold in plasmonic systems with gain," ACS Photonics **4**, 1003–1008 (2017).
[24]D. J. Trivedi, D. Wang, T. W. Odom, and G. C. Schatz, "Model for describing plasmonic nanolasers using Maxwell-Liouville equations with finite-difference time-domain calculations," Phys. Rev. A **96**, 053825 (2017).
[25]M. Richter, M. Gegg, T. S. Theuerholz, and A. Knorr, "Numerically exact solution of the many emitter–cavity laser problem: Application to the fully quantized spaser emission," Phys. Rev. B **91**, 035306 (2015).
[26]H.-P. Breuer and F. Petruccione, *The Theory of Open Quantum Systems* (Oxford University Press on Demand, 2002).
[27]H. J. Carmichael, *Statistical Methods in Quantum Optics 2: Non-Classical Fields* (Springer Science & Business Media, 2009).
[28]P. B. Johnson and R.-W. Christy, "Optical constants of the noble metals," Phys. Rev. B **6**, 4370 (1972).
[29]N. Nilius, N. Ernst, and H.-J. Freund, "Photon emission spectroscopy of individual oxide-supported silver clusters in a scanning tunneling microscope," Phys. Rev. Lett. **84**, 3994 (2000).